Article

Photothermal Response for the Thermoelastic Bending Effect Considering Dissipating Effects by Means of Fractional Dual-Phase-Lag Theory

Aloisi Somer [1],*, Andressa Novatski [1], Marcelo Kaminski Lenzi [2], Luciano Rodrigues da Silva [3,4] and Ervin Kaminski Lenzi [1,4]

1   Departamento de Física, Universidade Estadual de Ponta Grossa, Av. Gen. Carlos Cavalcanti 4748, Ponta Grossa 84030-900, PR, Brazil
2   Departamento de Engenharia Química, Universidade Federal do Paraná, Rua XV de Novembro, Curitiba 80060-000, PR, Brazil
3   Departamento de Física, Universidade Federal do Rio Grande do Norte, Natal 59078-900, RN, Brazil
4   National Institute of Science and Technology for Complex Systems, Centro Brasileiro de Pesquisas Físicas, Rio de Janeiro 22290-180, RJ, Brazil
*   Correspondence: asomer@uepg.br

Abstract: We analyze an extension of the dual-phase lag model of thermal diffusion theory to accurately predict the contribution of thermoelastic bending (TE) to the Photoacoustic (PA) signal in a transmission configuration. To achieve this, we adopt the particular case of Jeffrey's equation, an extension of the Generalized Cattaneo Equations (GCEs). Obtaining the temperature distribution by incorporating the effects of fractional differential operators enables us to determine the TE effects in solid samples accurately. This study contributes to understanding the mechanisms that contribute to the PA signal and highlights the importance of considering fractional differential operators in the analysis of thermoelastic bending. As a result, we can determine the PA signal's TE component. Our findings demonstrate that the fractional differential operators lead to a wide range of behaviors, including dissipative effects related to anomalous diffusion.

Keywords: anomalous diffusion; fractional dynamics; Generalized Cattaneo Equation

1. Introduction

The thermoelastic bending (TE) effect must be considered in photothermal measurements when the temperature change in the sample, due to light absorption, creates mechanical stress that leads to a non-uniform thermal displacement [1,2]. It must be carefully considered in the design and interpretation of photothermal experiments, as it can impact the accuracy of the results if not adequately accounted for [3,4]. Thin samples with significant heat expansion and materials with anisotropic thermal expansion are particularly susceptible to the TE effect. In addition, the TE effect is also essential in the analysis of the photothermal responses when thermal characteristics of solid materials are investigated using the Photoacoustic signal [5–23].

To accurately quantify the thermoelastic (TE) effect, we must determine the temperature distribution in the sample as a result of light absorption. This is obtained by solving the heat diffusion equation, which describes how heat is transferred through the material. The standard heat diffusion equation considers the thermal conductivity using the Fourier Law and the heat generation rate through the Energy Conservation Law [24,25]. For the photothermal techniques, the classical model does not consider heat loss, which can be due to convection and radiation, heat loss to edges, and non-homogeneity [2].

The thermoelastic bending effect and other dissipation effects in photothermal data can be modeled mathematically using fractional calculus [24–31]. It is worth mentioning that the fractional calculus enables the modeling of processes that are not characterized

by traditional (integer order) derivatives [26,29,32,33,33–41] and can be suitably used to analyze anomalous diffusion and viscoelasticity in many materials [42,43]. In these scenarios, the effects of memory and dissipation in the material can significantly impact temperature distribution, and the TE effect, which can be captured by modeling the heat transfer with fractional derivatives [26,27,44] and the mechanical reaction of the sample (viscoelastic), can also be analyzed using fractional calculus. Combining these methods with the fractional calculus enables modeling the mechanical response's time-dependent behavior in photothermal measurements, where the laser power and sample temperature are quickly changing [45–47].

Here, we apply an extension of dual phase lag in thermal systems to predict the PA signal's temperature distribution and TE component for transmission configuration. The extension is a new fractional operator derived from Jeffrey's equation, an extension of the GCE-I model with a fractional dual-phase-lag, considered to obtain the thermal piston component of the PA signal [48] and photothermal response in periodic heating [49]. We show that applying fractional calculus in photothermal measurements can offer a more detailed description of the complex and dynamic behavior of the system, resulting in a more accurate calculation of the TE effect and a more transparent comprehension of the physical processes.

2. Theory

The Fourier Law connects the heat flux, $\mathbf{q}(\mathbf{r}, t)$, at a given point in space and time is proportional to the temperature gradient, $\nabla T(\mathbf{r}, t)$, at that same point.

$$\mathbf{q}(\mathbf{r}, t) = -k \nabla T(\mathbf{r}, t) \tag{1}$$

where k is the thermal conductivity. It has been shown that fractional equations are a useful mathematical tool for describing the dynamics of a variety of odd physical events [50–52]. Compte and Metzeler [53] made phenomenological generalizations of the Cattaneo Equation [54]. In particular, we have the GCE-I generalization:

$$\left(1 + \tau_q^\alpha \partial_t^\alpha\right) \mathbf{q}(\mathbf{r}, t) = -k_\alpha \partial_t^{1-\alpha} \nabla T(\mathbf{r}, t) \tag{2}$$

The Jeffreys-type equation is a generalization for the study of the Fractional Dual-Phase-Lag (FDPL) [48]:

$$\left(1 + \tau_q^\alpha \partial_t^\alpha\right) \mathbf{q}(\mathbf{r}, t) = -k_\gamma \partial_t^{1-\gamma} \left(1 + \tau_T^\beta \partial_t^\beta\right) \nabla T(\mathbf{r}, t) \tag{3}$$

where $0 < \alpha, \beta, \gamma < 1$, and $k\gamma = k\tau_q^{1-\gamma}$, and ∂_t^α is the Caputo fractional derivative or integral, which are, respectively

$$_{t_0}\partial_t^\gamma f(x, t) = \begin{cases} \frac{1}{\Gamma(1-\gamma)} \int_{t_0}^t \frac{dt'}{(t-t')^\gamma} \frac{\partial}{\partial t} f(x, t'), & \text{for } 0 < \gamma < 1 \\ \frac{1}{\Gamma(-\gamma)} \int_{t_0}^t dt' \frac{f(x, t')}{(t-t')^{1+\gamma}}, & \text{for } \gamma < 0 \end{cases} \tag{4}$$

A special case of Jeffreys-type equation is for $\alpha = \gamma$, in which is obtained an extension of GCE-I Compte-Metzler equation with a Dual-Phase-Lag (FDPL-GCE-I):

$$\left(1 + \tau_q^\alpha \partial_t^\alpha\right) \mathbf{q}(\mathbf{r}, t) = -k_\alpha \partial_t^{1-\alpha} \left(1 + \tau_T^\beta \partial_t^\beta\right) \nabla T(\mathbf{r}, t) \tag{5}$$

Furthermore, the validity interval is generalized, following Jeffrey's equations, with $0 \leq \alpha, \beta \leq 1$. If $\beta = 1$ and $\tau_T = 0$ in Equation (5),

The thermal diffusion equation is obtained by combining the Fourier Law, Equation (1), with the Energy Conservation Law, which is:

$$\rho c_p \partial_t T(\mathbf{r}, t) + \nabla \cdot \mathbf{q}(\mathbf{r}, t) = F(\mathbf{r}, t) \tag{6}$$

with $F(\mathbf{r}, t)$, ρ, and c_p the heat source, density, and specific heat, respectively. The classical thermal diffusion (CTD) equation is

$$\nabla^2 T(\mathbf{r}, t) - \frac{1}{D}\partial_t T(\mathbf{r}, t) = -\frac{1}{k} F(\mathbf{r}, t) \,, \tag{7}$$

where the standard thermal diffusivity is defined as $D = k/\rho c_p$.

For the general case, from the Jeffreys-type equation, Equation (3), the thermal diffusion equation is:

$$\partial_t^{1-\gamma}\left(1 + \tau_T^\beta \partial_t^\beta\right)\nabla^2 T(\mathbf{r}, t) - \frac{1}{D_\gamma}\left(1 + \tau_q^\alpha \partial_t^\alpha\right)\partial_t T(\mathbf{r}, t) =$$
$$-\frac{1}{k_\gamma}\left(1 + \tau_q^\alpha \partial_t^\alpha\right) F(\mathbf{r}, t) \tag{8}$$

with the fractional thermal diffusivity defined as $D_\gamma = k_\gamma/\rho c_p$. For the FDPL-GCE-I the Thermal Diffusion Equation is obtained:

$$\left(1 + \tau_T^\beta \partial_t^\beta\right)\nabla^2 T(\mathbf{r}, t) - \frac{1}{D_\alpha}\partial_t^{\alpha-1}\left(1 + \tau_q^\alpha \partial_t^\alpha\right)\partial_t T(\mathbf{r}, t) =$$
$$-\frac{1}{k_\alpha}\partial_t^{\alpha-1}\left(1 + \tau_q^\alpha \partial_t^\alpha\right) F(\mathbf{r}, t) \tag{9}$$

The anomalous thermal conductivity k_α has dimensions $kg \cdot m \cdot s^{-2-\alpha} \cdot K^{-1}$ and the anomalous thermal diffusivity D_α has dimension $m^2 \cdot s^{-\alpha}$.

The Thermoelastic Bending Effect in Photoacoustic Signal

The Photoacoustic (PA) signal is a pressure variation recorded during PA measurements in the sample nearby gas. Figure 1 shows the geometry for the TE calculation, as in ref. [2,4]. The pressure variation δP_{TE} due to thermoelastic effect is [1]:

$$\delta P_{TE} = \frac{\Gamma P_0}{V_0} 2\pi \int_0^R r u_z(z = l_s/2, r, t) dr \tag{10}$$

where Γ is the air-specific heat ratio, P_0 is the atmospheric pressure, $u_z(z = l_s/2, r, t)$ is the displacement of the sample due to the heating, R is the radius of the sample, and $V_0 = \pi R_c l_g$ with R_c the cell radius.
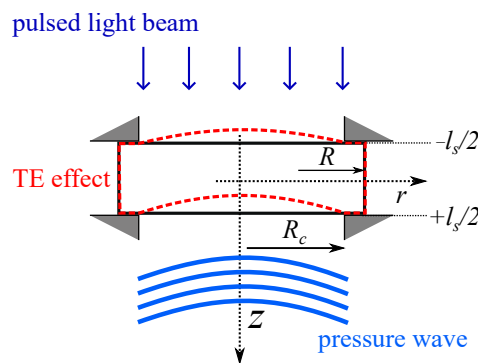
Figure 1. Geometry for the TE problem in photoacoustic transmission excitation of sample with thickness l_s and radius R by considering $R \gg l_s$. R_c is the PA cell radius.

The displacement $u_z(r, z)$ of a thin solid-plate approach is [3,25,55]:

$$u_z\left(r, \frac{l_s}{2}\right) = \alpha_T \frac{6(R^2 - r^2)}{l_s^3} M_T \tag{11}$$

where α_T is the thermal expansion coefficient, and $M_T = \int_{-l_s/2}^{l_s/2} zT_s(z)dz$ is the temperature gradient. To determine the temperature distribution, it is necessary to solve Equation (9). Therefore, it is assumed that the absorption of radiation by air is insignificant, thus the heat source is present exclusively within the sample:

$$F_s(z,t) = \eta_s I_0 \lambda_s e^{-\lambda_s z} e^{i\omega t} \,, \tag{12}$$

with $\omega = 2\pi f$, in which f is the frequency of light modulation, λ_s, I_0, and η_s are the optical absorption coefficient, the light intensity, and the quantum coefficient of the electromagnetic energy to heat conversion of the sample, respectively (it is considered that $\eta_s = 1$).

The photothermal signal (PA signal) is monitored with the same frequency as the heat source, requiring that the temperature variations in the three media (air-sample-air) have a similar waveform to the source. This temperature variation can be expressed as $T(z,t) = \theta(z)e^{i\omega t}$. Due to the experimental characteristics, we consider $t_0 = -\infty$. Thus, $\partial_t^\gamma e^{i\omega t} = (i\omega)^\gamma e^{i\omega t}$ [52]. Additionally, the photothermal analysis (PA) problem can be treated as a one-dimensional problem when the light-induced heating is uniform and covers an area larger than the sample's radius. In such cases, the temperature profile of the sample, $T_s(z,t)$, can be obtained by solving a set of one-dimensional heat diffusion equations. This assumption simplifies the analysis and provides a more straightforward method of understanding the temperature distribution within the sample:

$$\frac{d^2}{d\tilde{z}^2}\theta_j(z) - \frac{m_j}{D_{\alpha_j}}(i\omega)\theta_j(z) = -\frac{m_j}{k_{\alpha j}}F_j(z) \tag{13}$$

with $j = b, s, g$ for backing air, sample, and air closed in PA cell, respectively, and m_j is obtained from FDPL-GCE-I temporal fractional derivatives:

$$m_j = \frac{(i\omega)^{\alpha_j-1}\left(1 + \tau_{qj}^{\alpha_j}(i\omega)^{\alpha_j}\right)}{\left(1 + \tau_{Tj}^{\beta_j}(i\omega)^{\beta_j}\right)} \tag{14}$$

To solve, we considered the boundary conditions: (1) the zero temperature variation in system borders at $z = \pm\infty$, (2) continuity of temperature, and (3) continuity heat flux, both at the interfaces backing air-sample ($z = -l_s/2$), and sample-air inner the PA cell ($z = l_s/2$). Solving (13) and assuming that: (1) the thermal effusivity ($e = (k\rho c)^{1/2}$) of the sample is much greater than the air [56]; (2) the fractional order derivatives for air are $\alpha = \beta = 1$; and (3) the two relaxation times of air are small, $\tau_q \to 0$ and $\tau_T \to 0$, the temperature distribution is:

$$T_s(z,t) = \frac{I_0 \cosh\left(\sigma_{m_s}\left(z - \frac{l_s}{2}\right)\right)}{k_{m_s}\sinh(\sigma_{m_s}l_s)}H_s(z,\beta)e^{i\omega t} \,, \tag{15}$$

where $k_{m_s} = k_s/m_s$, $\sigma_{m_s} = m_s^{1/2}\sigma_s$, and σ_j is the complex medium thermal diffusion length, with $j = g, b$ for the surrounding air and $j = s$ for the sample, given by:

$$\sigma_j = \sqrt{\frac{i\omega}{D_j}}, \tag{16}$$

and $H_s(z,\beta) = \Lambda_1(z,\beta) - \Lambda_2(z,\beta)$ is the optical absorbing contribution, which tends to unit for opaque approach ($\lim_{\beta\to\infty} H_s(z,\beta) = 1$). The functions Λ_1 and Λ_2 are defined as follows:

$$\Lambda_1(z,\beta) = \frac{1 - e^{-\beta l_s}\cosh\left(\sigma_{m_s}\left(\frac{l_s}{2}+z\right)\right)\text{sech}\left(\sigma_{m_s}\left(z-\frac{l_s}{2}\right)\right)}{1-\frac{\sigma_{m_s}^2}{\beta^2}}, \tag{17}$$

$$\Lambda_2(z,\beta) = \frac{\sigma_{m_s}e^{-\beta\left(\frac{l_s}{2}+z\right)}\sinh(l_s\sigma_{m_s})\text{sech}\left(\sigma_{m_s}\left(z-\frac{l_s}{2}\right)\right)}{\beta\left(1-\frac{\sigma_{m_s}^2}{\beta^2}\right)}.$$

The GCE-I (One-Phase-Lag) presents a subdiffusive behavior for long timespans ($t < \tau_q$), i.e., in the high-frequency domain for photothermal techniques. It was obtained from phase velocity for the FDPL-GCE-I, which is mainly characterized by subdiffusive behavior, but the τ_T promotes the superdiffusive behavior mainly for high-frequency modulations [49]. The thermoelastic bending contribution δP_{TE} of the sample to the PA signal is

$$\delta P_{TE} = \frac{C_1 C_2 m_s\left(e^{-\beta l_s}+1\right)}{\sigma_{ms}^3\left(1-\frac{\sigma_{ms}^2}{\beta^2}\right)} \tag{18}$$

$$\times\left(F_{1s}-l_s\sigma_{ms}\left(1-\frac{\sigma_{ms}^2}{\beta^2}\right)+2\tanh\left(\frac{l_s\sigma_{ms}}{2}\right)\right)$$

where $F_{1s} = \frac{2\sigma_{\gamma s}^3\left(e^{-\beta l_s}-1\right)}{\beta^3\left(e^{-\beta l_s}+1\right)}$, where $C_1 = \frac{\Gamma I_0 P_0\sqrt{\alpha_g}}{\sqrt{2\pi}l_g T_0 k_s}$ is the amplitude of thermal diffusion contribution and its unit in the S.I is $[C_1] = $Pa m^{-1}s$^{-1/2}$, and $C_2 = \frac{3\sqrt{2\pi}R^4 T_0\alpha_T}{2R_c^2\sqrt{\alpha_g}l_s^3}$ is the relative amplitude of thermoelastic contribution, and your unit in the S.I is $[C_2]=$m^{-2}s$^{1/2}$ [45]. For the opaque approach ($\beta \to \infty$):

$$\delta P_{TE} = \frac{C_1 C_2 m_s\left(2\tanh\left(\frac{l_s\sigma_{ms}}{2}\right)-l_s\sigma_{m_s}\right)}{l_s^3\sigma_{ms}^3}. \tag{19}$$

Considering the classical thermal diffusion ($m = 1$), the PA signal tends to the equation determined by Rousset et al. [1].

3. Results and Discussion

The analytical results are obtained for an opaque sample of thickness $l_s = 400$ µm and thermal diffusivity $\alpha_s = 40\times10^{-6}$ m^2/s, as a function of fractional order derivatives α and β, heated by a uniform light source at $z = -l_s/2$. The temperature distribution was normalized by (k_s/I_0) to show how the factor m_s, and hence the fractional factor $alpha$, affect temperature distribution. Furthermore, the PA signal is normalized considering $C_1 C_2 = 1$. All simulations were performed until the establishment of attenuation for the subdiffusive behavior, which occurs around the $0.5 < \alpha < 1$ interval [49].

3.1. Temperature Distribution

Figure 2 shows the influence of the Dual-Phase-Lag in GCE-I on the absolute value of the temperature profile normalized. The temperature results are simulated as a function of position z and fractional order derivative heated by a uniform light source at $z = -l_s/2$ with frequency $f = 1000$ Hz. A particular case of FDPL-GCCE-I with $\alpha = \beta$ and $\tau_T = \tau_q$ is presented in Figure 2b.
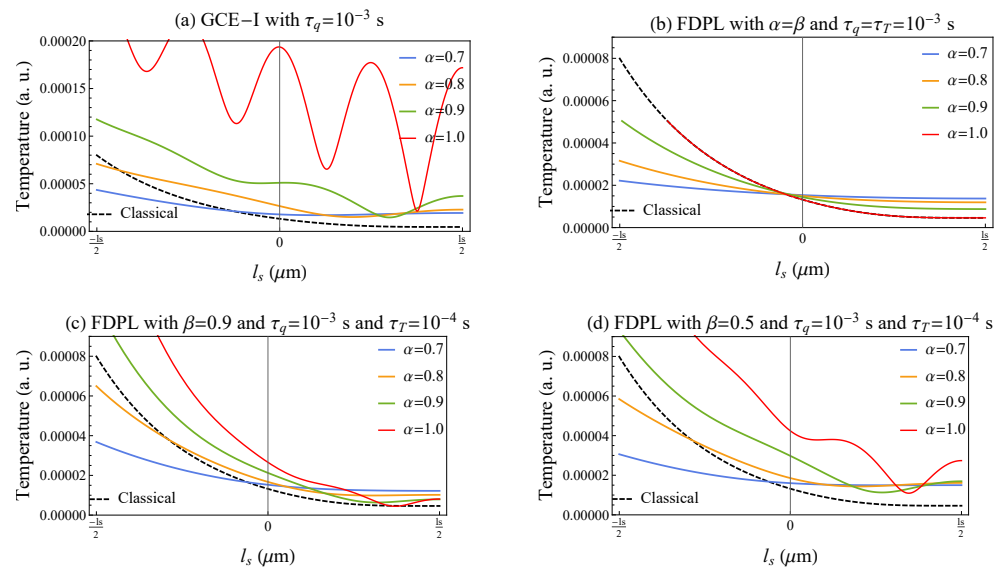
Figure 2. Normalized $(k_s T_s(z)/I_0)$ absolute value of the temperature distribution of an opaque sample heated by a light source at $z = -l_s/2$ in the function of (α) with $l_s = 400$ μm, $f = 1000$ Hz and $D_s = 40 \times 10^{-6}$ m^2/s for (**a**) GCE-I, and FDPL-GCE-I for (**b**) special case with $\alpha = \beta$, (**c**) $\beta = 0.9$, and (**d**) $\beta = 0.5$.

The graphical representation provides the peculiar characteristics that arise during heat wave propagation through the sample for each considered model. The following remarks can be highlighted

- The subdiffusive Generalized Continuous Equation of the First Kind (GCE-I) has been shown to reduce the resonant oscillations of the hyperbolic model and diminish the temperature gradient inside the sample. The attenuation of oscillations in the GCE-I model for photothermal excitations has been previously observed [23,45,57], as shown by the red curve in Figure 2a, given that the GCE-I model returns to the hyperbolic equation when $\alpha = 1$. Furthermore, a decrease in the value of α leads to a reduction in the temperature variation, which in turn affects the amplitude of the TE effect;

- The second Phase-Lag term functions as a damping factor for the resonant oscillations in the hyperbolic model but has the consequence of increasing the temperature gradient. By setting $\gamma = \alpha$ in Jeffrey's Equation (3), the resulting Equation (5) can be interpreted as a DPL extension of the GCE-I model. As illustrated in Figure 2c,d, the DPL parameters τ_q and β lead to a reduction in the resonant oscillations while simultaneously increasing the temperature in the region of incidence radiation ($z = -l_s/2$). The degree of attenuation is determined by the fractional order β, while the relaxation time τ_q is responsible for the variation in a temperature gradient. This is closer to real-world scenarios, as resonant oscillations are typically absent, but the TE effect induced by the temperature gradient is present and can be measured;

- In the scenario where the fractional order, β, and relaxation time, τ_T, are close to the values of α and τ_q, respectively, the damping of resonant oscillations is maximized, which is the strongest damping situation. Additionally, the temperature gradient exhibits a weaker behavior than that predicted by the classical and GCE-I models.

3.2. Photoacoustic Signal

Figure 3 presents the influence of the FDPL-GCE-I on the PA signal. Aside from analyzing the amplitude of the PA signal $|\delta P|$, as shown in the left column graphs (Figure 3a,c,e,g), it is also possible to analyze the phase delay ϕ_{PA} in which the signal is generated, as demonstrated in the right column graphs (Figure 3b,d,f,h). The strongest damping (particular case) with $\alpha = \beta$ and $\tau_q = \tau_T$ is analyzed in Figure 3c,d.
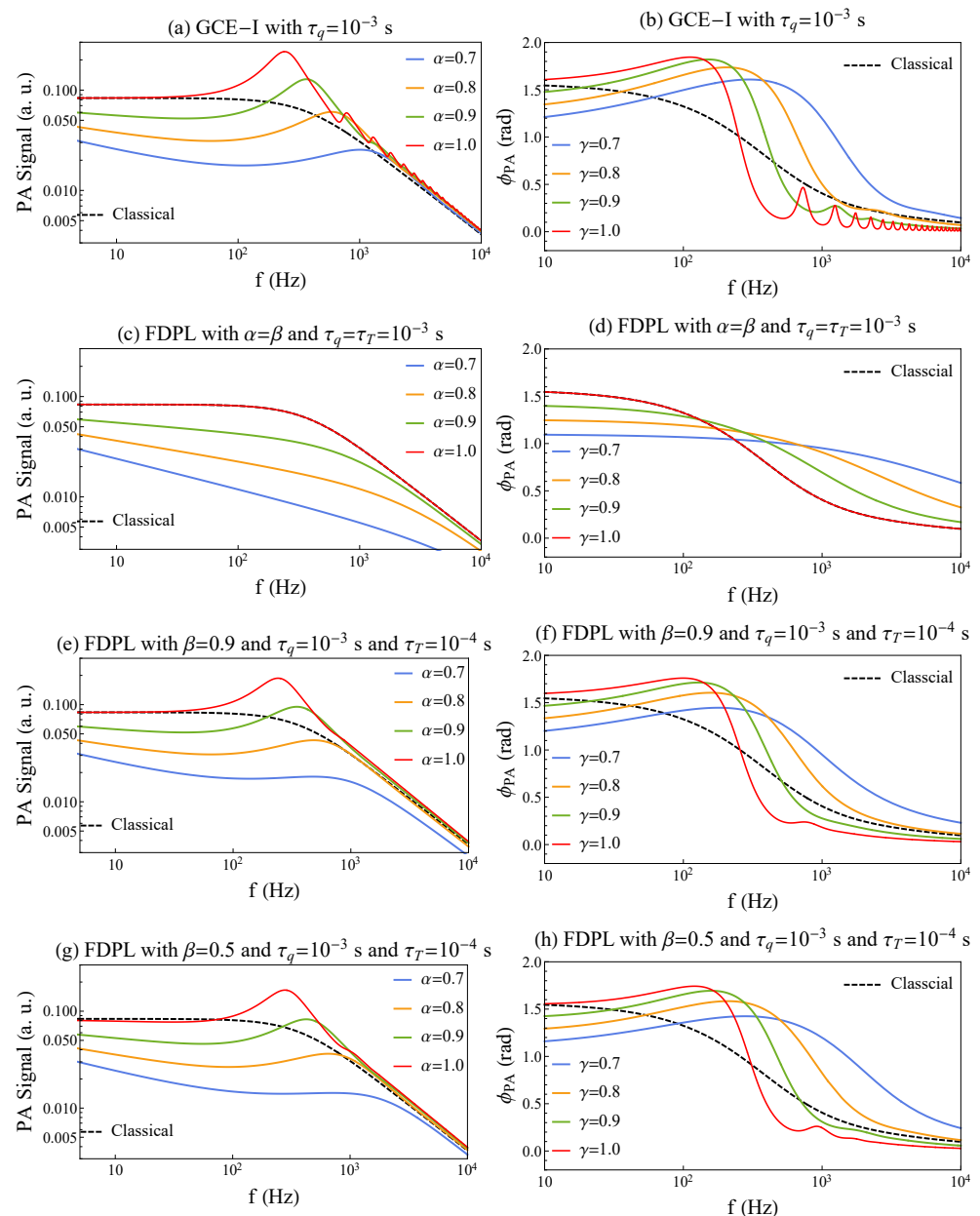
Figure 3. PA signal amplitude $|\delta P|$ in (**a**,**c**,**e**,**g**) and phase delay ϕ in (**b**,**d**,**f**,**h**) for FDPL-GCE-I as the function of frequency (f) and fractional derivative order (α) with $l_s = 400$ μm, $\alpha_s = 40 \times 10^{-6}$ m²/s and $\tau_q = 10^{-3}$ s.

The temperature gradient mostly strongly influences the pressure wave generated at each modulation frequency. The results of the PA signal due to the TE effect, which can be added to the discussion of temperature results, are:

- The GCE-I makes the amplitude tend the classical behavior to high frequencies increases the first resonant peak. On the other hand, the phase delay exhibits a sharp decrease around the first resonant peak, which shifts to higher frequencies as α decreases;
- For low α, the PA signal is lower than the classical result, even for higher frequencies. This situation can explain the strongest dissipating phenomena;
- The influence of the fractional derivative photothermal model FDPL-GCE-I on the amplitude of the photoacoustic (PA) signal is more prominent at lower frequencies. In contrast, its impact on the phase can be detected across the entire frequency range.

Specifically, the phase delay is more sensitive to anomalous effects, especially when detecting equipment works at high frequencies.

It is worth noting that when there is an inversion of the relaxation times, leaving $\tau_T > \tau_q$, a more intense attenuation occurs.

4. Conclusions

The FDPL-GCE-I equations were proposed to model the fractional heat conduction and thermal diffusion in materials by incorporating two fractional order derivatives and two relaxation times based on Jeffrey's model. We obtained an analytical solution for the temperature profile for a periodic photothermal excitation, assuming a homogeneous sample surrounded by air, which can be either transparent or opaque, to investigate the contribution of the thermoelastic (TE) effect to the photoacoustic (PA) problem.

The model exhibiting subdiffusive behavior for a broad range of modulation frequencies typical of photothermal techniques can provide insights into anomalous effects arising from anisotropic and dissipative effects that are not accounted for in classical and hyperbolic models. This model helps explain the underlying physics of these phenomena and can enhance our understanding of the dynamics of such complex systems.

Author Contributions: A.S.: Methodology, Investigation, writing—original draft preparation. A.N.: Supervision, writing—review and editing. M.K.L.: Validation, writing—review and editing. L.R.d.S.: Validation, writing—review and editing. E.K.L.: Conceptualization, Funding acquisition, Writing—review & editing. All authors have read and agreed to the published version of the manuscript.

Data Availability Statement: The data presented in this study are available on request from the corresponding author.

Conflicts of Interest: The authors declare no conflict of interest.

Abbreviations

The following abbreviations are used in this manuscript:

PA	Photoacoustic
TE	Thermoelastic Bending
GCE-I	Generalized Cattaneo Equation type I
DPL	Dual-Phase-Lag
FDPL	Fractional Dual-Phase-Lag
FDPL-GCE-I	Fractional Dual-Phase-Lag obtained from Jefrey's Equation interpreted as a dual-phase-lag extension of GCE-I

References

1. Rousset, G.; Lepoutre, F.; Bertrand, L. Influence of thermoelastic bending on photoacoustic experiments related to measurements of thermal diffusivity of metals. *J. Appl. Phys.* **1983**, *54*, 2383–2391. [CrossRef]
2. Perondi, L.F.; Miranda, L.C.M. Minimal-volume photoacoustic cell measurement of thermal diffusivity: Effect of the thermoelastic sample bending. *J. Appl. Phys.* **1987**, *62*, 2955–2959. [CrossRef]
3. Todorović, D.M. Plasmaelastic and thermoelastic waves in semiconductors. *J. Phys. IV Fr.* **2005**, *125*, 551–555. [CrossRef]
4. Aleksić, S.; Markushev, D.; Markushev, D.; Pantic, D.; Lukic, D.; Popovic, M.; Galovic, S. Photoacoustic Analysis of Illuminated Si-TiO$_2$ Sample Bending Along the Heat-Flow Axes. *Silicon* **2022**, *14*, 9853–9861. [CrossRef]
5. Somer, A.; Gonçalves, A.; Moreno, T.V.; Cruz, G.K.; Baesso, M.L.; Astrath, N.G.C.; Novatski, A. Photoacoustic signal with two heating sources: Theoretical predictions and experimental results for the Open Photoacoustic Cell technique. *Meas. Sci. Technol.* **2020**, *31*, 075202. [CrossRef]

6. Somer, A.; Camilotti, F.; Costa, G.; Bonardi, C.; Novatski, A.; Andrade, A.; Kozlowski, V., Jr.; Cruz, G. The thermoelastic bending and thermal diffusion processes influence on photoacoustic signal generation using open photoacoustic cell technique. *J. Appl. Phys.* **2013**, *114*, 063503. [CrossRef]

7. Somer, A.; Camilotti, F.; Costa, G.; Jurelo, A.; Assmann, A.; De Souza, G.; Cintho, O.; Bonardi, C.; Novatski, A.; Cruz, G. Effects of thermal oxidation on the effective thermal diffusivity of titanium alloys. *J. Phys. D Appl. Phys.* **2014**, *47*, 385306. [CrossRef]

8. Markushev, D.K.; Markushev, D.D.; Aleksić, S.M.; Pantić, D.S.; Galović, S.P.; Todorović, D.M.; Ordonez-Miranda, J. Experimental photoacoustic observation of the photogenerated excess carrier influence on the thermoelastic response of n-type silicon. *J. Appl. Phys.* **2020**, *128*, 095103. [CrossRef]

9. Jovančić, N.; Markushev, D.; Markushev, D.; Aleksić, S.; Pantic, D.; Korte, D.; Franko, M. Thermal and Elastic Characterization of Nanostructured Fe_2O_3 Polymorphs and TiO_2-Coated Fe_2O_3 Using Open Photoacoustic Cell. *Int. J. Thermophys.* **2020**, *41*, 90. [CrossRef]

10. Astrath, F.B.G.; Astrath, N.; Baesso, M.; Bento, A.; Moraes, J.C.S.; Santos, A. Open photoacoustic cell for thermal diffusivity measurements of a fast hardening cement used in dental restoring. *J. Appl. Phys.* **2012**, *111*, 014701. [CrossRef]

11. Souza, S.; Trichês, D.; Poffo, C.; De Lima, J.; Grandi, T.; De Biasi, R. Structural, thermal, optical, and photoacoustic study of nanocrystalline Bi_2Te_3 produced by mechanical alloying. *J. Appl. Phys.* **2011**, *109*, 013512. [CrossRef]

12. Markushev, D.D.; Ordonez-Miranda, J.; Rabasović, M.D.; Chirtoc, M.; Todorović, D.M.; Bialkowski, S.E.; Korte, D.; Franko, M. Thermal and elastic characterization of glassy carbon thin films by photoacoustic measurements. *Eur. Phys. J. Plus* **2017**, *132*, 33. [CrossRef]

13. Todorovic, D.; Rabasovic, M.; Markushev, D.; Jovic, V.; Radulovic, K.; Sarajlic, M. Photoacoustic Elastic Bending Method: Characterization of Thin Films on Silicon Membranes. *Int. J. Thermophys.* **2015**, *36*, 1016–1028. [CrossRef]

14. Nesic, M.; Popovic, M.; Djordjevic, K.; Miletić, V.; Jordovic Pavlovic, M.; Markushev, D.; Galovic, S. Development and comparison of the techniques for solving the inverse problem in photoacoustic characterization of semiconductors. *Opt. Quantum Electron.* **2021**, *53*, 381. [CrossRef]

15. Djordjevic, K.; Galovic, S.; Jordovic Pavlovic, M.; Nesic, M.; Popovic, M.; Cojbasic, Z.; Markushev, D. Photoacoustic optical semiconductor characterization based on machine learning and reverse-back procedure. *Opt. Quantum Electron.* **2020**, *52*, 247. [CrossRef]

16. Nesic, M.; Popovic, M.; Rabasovic, M.; Milicevic, D.; Suljovrujic, E.; Markushev, D.; Stojanovic, Z. Thermal Diffusivity of High-Density Polyethylene Samples of Different Crystallinity Evaluated by Indirect Transmission Photoacoustics. *Int. J. Thermophys.* **2017**, *39*, 24. [CrossRef]

17. Herrmann, K.; Pech-May, N.; Retsch, M. Photoacoustic thermal characterization of low thermal diffusivity thin films. *Photoacoustics* **2021**, *22*, 100246. [CrossRef]

18. Nesic, M.; Popovic, M.; Galovic, S.; Djordjevic, K.; Jordovic Pavlovic, M.; Miletić, V.; Markushev, D. Estimation of linear expansion coefficient and thermal diffusivity by photoacoustic numerical self-consistent procedure. *J. Appl. Phys.* **2022**, *131*, 105104. [CrossRef]

19. Markushev, D.; Markushev, D.; Aleksić, S.; Pantic, D.; Galovic, S.; Lukic, D.; Ordonez-Miranda, J. Enhancement of the thermoelastic component of the photoacoustic signal of silicon membranes coated with a thin TiO2 film. *J. Appl. Phys.* **2022**, *131*, 085105. [CrossRef]

20. Djordjevic, K.; Milicevic, D.; Galovic, S.; Suljovrujic, E.; Jacimovski, S.; Furundzic, D.; Popovic, M. Photothermal Response of Polymeric Materials Including Complex Heat Capacity. *Int. J. Thermophys.* **2022**, *43*, 68. [CrossRef]

21. Galović, S.; Kostoski, D. Photothermal wave propagation in media with thermal memory. *J. Appl. Phys.* **2003**, *93*, 3063–3070. [CrossRef]

22. Popovic, M.N.; Nesic, M.V.; Zivanov, M.; Markushev, D.D.; Galovic, S.P. Photoacoustic response of a transmission photoacoustic configuration for two-layer samples with thermal memory. *Opt. Quantum Electron.* **2018**, *50*, 330. [CrossRef]

23. Popovic, M.; Markushev, D.; Nesic, M.; Jordovic Pavlovic, M.; Galovic, S. Optically induced temperature variations in a two-layer volume absorber including thermal memory effects. *J. Appl. Phys.* **2021**, *129*, 015104. [CrossRef]

24. Youssef, H.M.; Al-Lehaibi, E.A. Fractional order generalized thermoelastic half-space subjected to ramp-type heating. *Mech. Res. Commun.* **2010**, *37*, 448–452. [CrossRef]

25. Song, Y.Q.; Bai, J.T.; Ren, Z.Y. Study on the reflection of photothermal waves in a semiconducting medium under generalized thermoelastic theory. *Acta Mech.* **2012**, *223*, 1545–1557. [CrossRef]

26. Hobiny, A.; Abbas, I. Fractional Order GN Model on Photo-Thermal Interaction in a Semiconductor Plane. *Silicon* **2019**, *12*, 1957–1964. [CrossRef]

27. Mondal, S.; Sur, A. Photo-thermo-elastic wave propagation in an orthotropic semiconductor with a spherical cavity and memory responses. *Waves Random Complex Media* **2021**, *31*, 1835–1858. [CrossRef]

28. Ignaczak, J.; Ostoja-Starzewski, M. *Thermoelasticity with Finite Wave Speeds*; Oxford Mathematical Monographs; Oxford University Press: Oxford, UK, 2009.

29. Ezzat, M.A.; El-Karamany, A.S.; Fayik, M.A. Fractional Ultrafast Laser–Induced Thermo-Elastic Behavior In Metal Films. *J. Therm. Stress.* **2012**, *35*, 637–651. [CrossRef]

30. Ezzat, M.A.; El-Karamany, A.S.; El-Bary, A.A.; Fayik, M.A. Fractional calculus in one-dimensional isotropic thermo-viscoelasticity. *Comptes Rendus Mécanique* **2013**, *341*, 553–566. [CrossRef]

31. Alaimo, G.; Piccolo, V.; Chiappini, A.; Ferrari, M.; Zonta, D.; Deseri, L.; Zingales, M. Fractional-Order Theory of Thermoelasticicty. I: Generalization of the Fourier Equation. *J. Eng. Mech.* **2018**, *144*, 04017164. [CrossRef]

32. Block, A.; Liebel, M.; Yu, R.; Spector, M.; Sivan, Y.; García de Abajo, F.J.; van Hulst, N.F. Tracking ultrafast hot-electron diffusion in space and time by ultrafast thermomodulation microscopy. *Sci. Adv.* **2019**, *5*, eaav8965. [CrossRef] [PubMed]

33. Koh, Y.R.; Shirazi-HD, M.; Vermeersch, B.; Mohammed, A.M.S.; Shao, J.; Pernot, G.; Bahk, J.H.; Manfra, M.J.; Shakouri, A. Quasi-ballistic thermal transport in $Al_{0.1}Ga_{0.9}N$ thin film semiconductors. *Appl. Phys. Lett.* **2016**, *109*, 243107. [CrossRef]

34. Mozafarifard, M.; Toghraie, D. Time-fractional subdiffusion model for thin metal films under femtosecond laser pulses based on Caputo fractional derivative to examine anomalous diffusion process. *Int. J. Heat Mass Transf.* **2020**, *153*, 119592. [CrossRef]

35. Lotfy, K.; El-Bary, A.A.; Tantawi, R.S. Effects of variable thermal conductivity of a small semiconductor cavity through the fractional order heat-magneto-photothermal theory. *Eur. Phys. J. Plus* **2019**, *134*, 280. [CrossRef]

36. Yasein, M.; Lotfy, K.; Mabrouk, N.; El-Bary, A.A.; Hassan, W. Response of Thermo- Electro-Magneto Semiconductor Elastic Medium to Photothermal Excitation Process with Thomson Influence. *Silicon* **2020**, *12*, 2789–2798. [CrossRef]

37. Wellershoff, S.S.; Hohlfeld, J.; Güdde, J.; Matthias, E. The role of electron–phonon coupling in femtosecond laser damage of metals. *Silicon* **1999**, *69*, S99–S107.

38. Nikbakht, M. Radiative heat transfer in fractal structures. *Phys. Rev. B* **2017**, *96*, 125436. [CrossRef]

39. Xu, H.Y.; Jiang, X.Y. Time fractional dual-phase-lag heat conduction equation. *Chin. Phys. B* **2015**, *24*, 034401. [CrossRef]

40. Xu, H.; Wang, X.; Qi, H. Fractional dual-phase-lag heat conduction model for laser pulse heating. In Proceedings of the 2017 29th Chinese Control and Decision Conference (CCDC), Chongqing, China, 28–30 May 2017; pp. 7833–7837.

41. Somer, A.; Galovic, S.; Lenzi, E.; Novatski, A.; Djordjevic, K. Temperature profile and thermal piston component of photoacoustic response calculated by the fractional dual-phase-lag heat conduction theory. *Int. J. Heat Mass Transf.* **2023**, *203*, 123801. [CrossRef]

42. Pękalski, A.; Sznajd-Weron, K. *Anomalous Diffusion: From Basics to Applications*; Springer: Berlin/Heidelberg, Germany, 1999.

43. Klafter, J.; Blumen, A.; Shlesinger, M.F. Stochastic pathway to anomalous diffusion. *Phys. Rev. A* **1987**, *35*, 3081. [CrossRef]

44. Hobiny, A.; Alzahrani, F.; Abbas, I. Analytical estimation of temperature in living tissues using the tpl bioheat model with experimental verification. *Mathematics* **2020**, *8*, 1188. [CrossRef]

45. Somer, A.; Novatski, A.; Lenzi, E.K. Theoretical predictions for photoacoustic signal: Fractionary thermal diffusion with modulated light absorption source. *Eur. Phys. J. Plus* **2019**, *134*, 18. [CrossRef]

46. Somer, A.; Novatski, A.; Carlos Serbena, F.; Kaminski Lenzi, E. Fractional GCEs behaviors merged: Prediction to the photoacoustic signal obtained with subdiffusive and superdiffusive operators. *J. Appl. Phys.* **2020**, *128*, 075107. [CrossRef]

47. Somer, A.; Novatski, A.; Serbena, F.C.; Lenzi, E.K. Interplay between super and subdiffusive behaviors in photothermal phenomena. *Int. J. Therm. Sci.* **2021**, *159*, 106539. [CrossRef]

48. Awad, E.; Sandev, T.; Metzler, R.; Chechkin, A. From continuous-time random walks to the fractional Jeffreys equation: Solution and properties. *Int. J. Heat Mass Transf.* **2021**, *181*, 121839. [CrossRef]

49. Somer, A.; Novatski, A.; da Silva, L.R.; Lenzi, M.; Novatski, A.; Lenzi, E. Fractional Dual-Phase-Lag Heat Conduction with Periodic Heating and Photothermal Response. *Thermal Sci.* **2023**, *accepted for publication*.

50. Lenzi, E.K.; Mendes, R.S.; Fa, K.S.; Moraes, L.S.; da Silva, L.R.; Lucena, L.S. Nonlinear fractional diffusion equation: Exact results. *J. Math. Phys.* **2005**, *46*, 083506. [CrossRef]

51. Evangelista, L.R.; Lenzi, E.K. *An Introduction to Anomalous Diffusion and Relaxation*; Springer Nature: Berlin/Heidelberg, Germany, 2023.

52. Evangelista, L.R.; Lenzi, E.K. *Fractional Diffusion Equations and Anomalous Diffusion*; Cambridge University Press: Cambridge, UK, 2018.

53. Compte, A.; Metzler, R. The generalized Cattaneo equation for the description of anomalous transport processes. *J. Phys. A Math. Gen.* **1997**, *30*, 7277–7289. [CrossRef]

54. Cattaneo, C. Sulla Conduzione del Calore. *Atti Sem. Mat. Fis. Univ. Modena* **1948**, *3*, 83–101.

55. Nesic, M.; Galovic, S.; Soskic, Z.; Popovic, M.; Todorovic, D.M. Photothermal Thermoelastic Bending for Media with Thermal Memory. *Int. J. Thermophys.* **2012**, *33*, 2203–2209. [CrossRef]

56. Rosencwaig, A.; Gersho, A. Theory of the photoacoustic effect with solids. *J. Appl. Phys.* **1976**, *47*, 64–69. [CrossRef]

57. Somer, A.; Popovic, M.N.; da Cruz, G.K.; Novatski, A.; Lenzi, E.K.; Galovic, S.P. Anomalous Thermal Diffusion in Two-Layer System: The Temperature Profile and Photoacoustic Signal for Rear Light Incidence. *Int. J. Therm. Sci.* **2022**, *179*, 107661. [CrossRef]